

Meta-generalized gradient approximation made in the Hartree gauge

Yan Oueis,^{1,*} Akilan Ramasamy,^{1,*} James W. Furness,^{1, a)} Jamin Kidd,¹ Timo Lebeda,¹ and Jianwei Sun^{1,†}

¹*Department of Physics and Engineering Physics,
Tulane University, New Orleans, LA 70118, USA*

a) Current address: Schrödinger, Inc., New York City, New York 10036, USA

(Dated: March 13, 2026)

In density functional theory (DFT), exact constraints, fundamental mathematical properties of the exchange-correlation (XC) energy and its underlying XC hole, along with paradigm systems such as the uniform electron gas and the hydrogen atom have been instrumental in developing exchange-correlation (XC) density functional approximations (DFAs). However, since the spatial XC energy density is not uniquely defined, its exact constraints can only be formulated within a chosen gauge and are therefore seldom utilized in DFA construction. Here, we propose a meta-generalized gradient approximation for the exchange energy, explicitly constructed within the Hartree gauge, using the hydrogen atom’s exchange energy density for gauge alignment in core and asymptotic regions. By formulating DFAs at the XC energy density level, this approach expands reference datasets for machine learning and establishes a foundation for more accurate nonlocal density functionals requiring gauge alignment.

INTRODUCTION

Due to its balance of accuracy and computational efficiency, density functional theory (DFT) [1, 2] has been widely used as a major electronic structure method across chemistry, materials science, and condensed matter physics [3–7]. While DFT is exact in principle for ground-state properties, practical use in the Kohn-Sham (KS) scheme requires approximating the exchange-correlation (XC) energy as a functional of the electron density. Significant progress has been made in developing density functional approximations (DFAs), from local spin density approximation (LSDA) [2, 8, 9], to generalized gradient approximation (GGA) [10–13], to meta-GGA (mGGA) [14–25], and to hybrid density functionals [26–33]. This evolution has largely been driven by the systematic incorporation of exact constraints, fundamental mathematical properties of the XC energy and its underlying XC hole density, that improve accuracy. For example, LSDA’s success stems from satisfying exact XC hole constraints [8, 34], while GGAs like the Perdew-Burke-Ernzerhof (PBE) functional [10] and mGGAs like the strongly constrained and appropriately normed (SCAN) density functional [20] were developed to fulfill additional exact constraints. Other successful density functionals [16, 21, 27, 30, 31, 33, 35] have been developed using total energy reference datasets.

Despite these advances, significant challenges such as self-interaction errors [36–41] and strong correlation [42–46] persist, often requiring nonlocal treatments. However, aligning nonlocal corrections with semilocal DFAs, especially GGAs and mGGAs, remains difficult due to the gauge ambiguity of the XC energy density [47]. This mismatch complicates the development of nonlocal functionals, as seen in local hybrid density functionals [36, 48, 49] and self-interaction corrections [38, 39, 50]. Addressing these issues requires modeling DFAs within

a specific gauge, the Hartree gauge (HG) [51]. This approach not only facilitates the development of nonlocal density functionals through gauge alignment but also enables producing extensive reference XC energy density datasets for machine learning applications.

The Becke-88 (B88) [12] exchange GGA recovers the correct asymptotic behavior of the exact exchange energy density in HG. It also recovers the second-order gradient expansion of the exchange energy with a coefficient approximately twice the first-principles value, resulting in poor performance for extended systems like jellium surfaces.

Here, we propose an exchange mGGA, called SORFKL, explicitly constructed in HG while maximally satisfying exact constraints of the exact exchange energy. SORFKL recovers the exact exchange HG energy density for the uniform electron gas (UEG) and closely matches it for the hydrogen atom, thus restoring the exact exchange HG energy density for the asymptotic and core regions of molecules and solids. The parameters of SORFKL are then fixed by appropriate norms, specifically the exchange energies of rare-gas atoms and jellium surfaces, following SCAN’s design strategy. Restoring the asymptotic and core regions of the exact exchange HG energy density and guided by exact constraints and appropriate norms, SORFKL provides an accurate representation of the exact exchange HG energy density for molecules at equilibrium with diverse bonding characteristics.

The exact exchange energy as a functional of the electronic density $n(\mathbf{r})$ is uniquely defined and can be expressed as

$$E_x^{\text{exact}}[n] = -\frac{1}{2} \int d\mathbf{r} \int d\mathbf{r}' \frac{|\rho_1(\mathbf{r}, \mathbf{r}')|^2}{|\mathbf{r} - \mathbf{r}'|}, \quad (1)$$

where $\rho_1(\mathbf{r}, \mathbf{r}') = \sum_i^{\text{occ}} \phi_i^*(\mathbf{r}) \phi_i(\mathbf{r}')$ is the one-electron reduced density matrix defined by the occupied KS orbitals $\{\phi_i[n](r)\}$. In contrast, the exchange energy den-

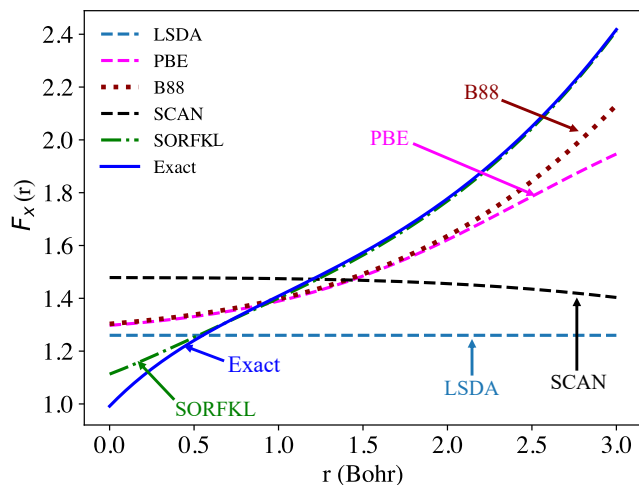


FIG. 1. Exchange enhancement factor of the hydrogen atom for different density functionals including LSDA, PBE, B88, SCAN, and SORFKL, and the exact exchange. The analytical electron density of the hydrogen atom is used. The corresponding exchange energies in Hartree are -0.2680 (LSDA), -0.3059 (PBE), -0.3098 (B88), -0.3125 (SCAN), -0.3125 (SORFKL), and -0.3125 (Exact).

sity $e_x^{\text{exact}}(\mathbf{r})$ is *not* unique. In fact, any nontrivial gauge transformation $e_x^{\text{exact}}(\mathbf{r}) \mapsto e_x^{\text{exact}}(\mathbf{r}) + G(\mathbf{r})$ with $\int d\mathbf{r}G(\mathbf{r}) = 0$ changes $e_x^{\text{exact}}(\mathbf{r})$ but not $E_x^{\text{exact}}[n]$. A particularly important gauge is the HG, in which $e_x^{\text{exact}}(\mathbf{r})$ corresponds directly to half of the electrostatic potential from the exchange hole,

$$e_x^{\text{exact}}(\mathbf{r}) = \frac{1}{2}n(\mathbf{r}) \int d\mathbf{r}' \frac{n_x(\mathbf{r}, \mathbf{r}')}{|\mathbf{r} - \mathbf{r}'|}. \quad (2)$$

The exchange hole $n_x(\mathbf{r}, \mathbf{r}') = -|\rho_1(\mathbf{r}, \mathbf{r}')|^2/n(\mathbf{r})$ is a component of the XC hole, whose system average is uniquely defined and an observable [52]. Semilocal DFAs can produce accurate exchange energies for systems with localized exchange holes, whereas they typically yield too negative exchange energies for systems with a delocalized hole [20]. Thus, comparing a semilocal exchange energy density, if constructed in HG, with the exact exchange HG energy density can, in principle, reveal whether the underlying exact exchange hole is localized or delocalized, an essential insight for developing nonlocal density functionals [36]. However, since the exchange energy densities of semilocal DFAs, $e_x^{\text{sl}}(\mathbf{r})$, are usually not in the HG [53], a direct comparison between $e_x^{\text{sl}}(\mathbf{r})$ and $e_x^{\text{exact}}(\mathbf{r})$ is of limited significance. In contrast, for a semilocal DFA constructed in HG, such as SORFKL, the ratio $e_x^{\text{sl}}(\mathbf{r})/e_x^{\text{exact}}(\mathbf{r})$ can reliably indicate whether the underlying exact exchange hole is localized.

For a spin-unpolarized UEG, a cornerstone in almost all DFAs, the exchange energy density is given by $e_x^{\text{uni}}(\mathbf{r}) = -\frac{3}{4\pi}(3\pi^2)^{1/3}n(\mathbf{r})^{4/3}$. In HG, the enhancement factor of exact exchange is $F_x^{\text{exact}}(\mathbf{r}) = e_x^{\text{exact}}(\mathbf{r})/e_x^{\text{uni}}(\mathbf{r})$,

while for a semilocal DFA, typically not in HG, the exchange enhancement factor is $F_x^{\text{sl}}(\mathbf{r}) = e_x^{\text{sl}}(\mathbf{r})/e_x^{\text{uni}}(\mathbf{r})$.

Upon assumption of local UEG behavior, the LSDA exchange DFA integrates $e_x^{\text{uni}}(\mathbf{r})$ over all space, followed by spin-scaling [54]. LSDA is in HG, as its energy density originates from the UEG exchange hole. However, due to its neglect of electron density inhomogeneity, LSDA is a poor approximation for inhomogeneous systems. Consequently, its enhancement factor significantly deviates from the exact exchange enhancement factor of the hydrogen atom (H) in HG, as shown in Fig. 1.

Alongside the UEG, the hydrogen atom serves as another paradigm system, with its electronic structure forming the foundation of much of chemistry. Specifically, the ground state of H, i.e., the 1s orbital, largely dictates the behavior of core electrons in molecules and solids. Accurately restoring the exact exchange HG energy density of H is therefore essential for developing exchange density functional approximations in HG for the core regions of both molecules and solids.

As shown in Fig. 1, no semilocal DFA to date has successfully recovered the exact exchange HG energy density of H. The B88 exchange GGA significantly improves over LSDA but still substantially deviates from the exact exchange HG enhancement factor. Meanwhile, the SCAN exchange mGGA [20], although satisfying all six exact constraints suitable for semilocal exchange, deviates from the exact HG exchange enhancement factor of H even more than LSDA, indicating that SCAN is constructed in a gauge fundamentally different from the HG.

Remarkably, the SORFKL exchange enhancement factor closely matches the exact exchange HG enhancement factor of H, as shown in Fig. 1. The SORFKL exchange energy for a spin-unpolarized electron density $n(\mathbf{r})$ is defined as

$$E_x^{\text{SORFKL}}[n] = \int d\mathbf{r} e_x^{\text{uni}}(n) F_x^{\text{SORFKL}}(s, \beta), \quad (3)$$

where $F_x^{\text{SORFKL}}(s, \beta)$ is a function of the reduced density gradient $s = |\nabla n|/(2(3\pi)^{1/3}n^{4/3})$ and the iso-orbital indicator $\beta = (\tau - \tau^{\text{vW}})/(\tau + \tau^{\text{uni}})$ that identifies different chemical environments, with the range $0 \leq \beta \leq 1$. The positive kinetic energy density of occupied KS orbitals is $\tau = \frac{1}{2} \sum_{i=1}^{\text{occ}} |\nabla \phi_i|^2$, which reduces to $\tau^{\text{vW}} = |\nabla n|^2/8n$ in single-orbital systems ($\beta = 0$) and to $\tau^{\text{uni}} = (3/10)(3\pi^2)^{2/3}n^{5/3}$ for a UEG ($\beta = 1/2$). In non-covalent bonds, $\beta \gg 1/2$ [55, 56]. We choose β over the related iso-orbital indicator $\alpha = (\tau - \tau^{\text{vW}})/\tau^{\text{uni}}$ that can also identify different chemical environments [20, 55, 57] due to β 's inherent numerical stability [56]. The exchange energy of spin-polarized electron densities can be obtained by applying the exact spin-scaling relation [54].

$F_x^{\text{SORFKL}}(s, \beta)$ is based on a model derived from the

exact exchange HG energy density of the hydrogen atom,

$$F_x^{\text{Hyd}}(s) = (3s)^{-2} \left[\frac{2}{3} \frac{(s/s_0)^3 - 1}{\ln(s/s_0)} - 1 \right], \quad (4)$$

where $s_0 = (6\pi)^{-1/3}$ is the smallest value of s in H, occurring at the nucleus (for details see the Supplemental Material [58], see also the references [59],[60],[12] therein). As $F_x^{\text{Hyd}}(s)$ can be negative for $s < s_0$ and even diverges as $s \rightarrow 0$, it is not suitable as a general model for exchange. Nevertheless, using $F_x^{\text{Hyd}}(s)$ as a framework provides several advantages. First, $F_x^{\text{Hyd}}(s)$ naturally recovers the asymptotic behavior of the exact HG exchange energy density per particle $\varepsilon_x^{\text{exact}} = e_x^{\text{exact}}/n$ for finite systems, $\lim_{r \rightarrow \infty} \varepsilon_x^{\text{exact}}(\mathbf{r}) \sim -\frac{1}{2r}$, by satisfying $\lim_{s \rightarrow \infty} F_x^{\text{Hyd}}(s) = (4\pi/9) \frac{s}{\ln(s)}$, a condition also built into the B88 GGA. Furthermore, the core electrons of molecules and materials are dominated by the 1s orbitals that closely resemble the ground state 1s orbital of the hydrogen atom. Thus, designing a semilocal DFA that recovers $F_x^{\text{Hyd}}(s)$ for the core and asymptotic regions ensures gauge alignment with the exact exchange HG energy density in those regions.

To keep the desired features of $F_x^{\text{Hyd}}(s)$ and at the same time remove its unphysical behavior for $s < s_0$, we replace s in Eq. (4) with a parameterizable function $g(s, \beta)$,

$$F_x^{\text{SORFKL}}(s, \beta) = F_x^{\text{Hyd}}(g(s, \beta)), \quad (5)$$

where

$$g(s, \beta) = \left[\frac{\sum_{i=0}^{N-1} a_i(\beta) s^{2i} + a_N s^{2N}}{\sum_{i=0}^{N-2} b_i(\beta) s^{2i} + a_N s^{2(N-1)}} \right]^{1/2} \quad (6)$$

depends on β through coefficients $\{a_i(\beta)\}$ and $\{b_i(\beta)\}$,

$$a_i(\beta) = \sum_{j=0}^M a_{ij} (1 - 2\beta)^j \text{ for } i = 0 \dots N - 1, \quad (7)$$

$$b_i(\beta) = \sum_{j=0}^M b_{ij} (1 - 2\beta)^j \text{ for } i = 0 \dots N - 2. \quad (8)$$

We find that $N = 2$ and $M = 2$ provides sufficient flexibility for this work. Without loss of generality, $b_{00} = 1$.

We demand a_N to be independent of β such that $\lim_{s \rightarrow \infty} g(s, \beta) = s$. Thus, $\lim_{s \rightarrow \infty} F_x^{\text{SORFKL}}(s, \beta) = \lim_{s \rightarrow \infty} F_x^{\text{Hyd}}(s)$ recovers the correct asymptotic behavior for finite systems. Additionally, this makes $F_x^{\text{SORFKL}}(s, \beta)$ only weakly dependent on β for large s , a common feature of successful mGGAs [15, 20, 25, 61].

In iso-orbital regions ($\beta = 0$), we demand $g(s, \beta = 0) \simeq s$ for $s > s_0$ such that $F_x^{\text{SORFKL}}(s, \beta = 0)$ recovers $F_x^{\text{Hyd}}(s)$ particularly for H.

At the center of two identical, infinitely separated closed shell atoms $s = 0$, $\beta \rightarrow 1$, and $F_x^{\text{exact}} \rightarrow \infty$, since

this is also the asymptotic region of this system, with respect to the nuclei where electron densities concentrate. To recover this condition we let the denominator of Equation (6) to zero for ($s = 0$, $\beta = 1$) by (using $b_{00} = 1$)

$$b_{01} = b_{02} + 1. \quad (9)$$

For the H_2^+ molecular ion, $\beta = 0$ everywhere and, due to symmetry, $s = 0$ at the bond center, regardless of the bond length R . In the limit $R \rightarrow 0^+$, where the two protons are maximally compressed, the electron density reduces to the hydrogenic 1s orbital density of He^+ . The latter has the same exact exchange HG enhancement factor as H. This indicates that F_x^{exact} at the bond center of H_2^+ in the limit $R \rightarrow 0^+$ equals that of H at the nuclear center. We demonstrate this numerically in the Supplemental [58] (see also the references [62], [17] therein). Consequently, we demand $F_x^{\text{SORFKL}}(s = 0, \beta = 0) = F_x^{\text{Hyd}}(s_0)$. Using Eq. (9) and $b_{00} = 1$, this condition leads to

$$a_{00} + a_{01} + a_{02} = 2b_{01}s_0^2. \quad (10)$$

For the slowly varying density limit, i.e., $\beta(\mathbf{r}) \rightarrow 1/2$ and $s \rightarrow 0$, we recover the second-order gradient expansion for the exchange energy. This fixes the coefficient $a_{00} = 0.2948$ and relates a_{01} , a_{10} , a_2 , and b_{01} by

$$\frac{a_2}{b_{00}} = \frac{a_{10}}{a_{00}} - \frac{20}{81 C_2} - \frac{65}{54} \left(\frac{b_{01}}{b_{00}} - \frac{a_{01}}{a_{00}} \right), \quad (11)$$

with $C_2 = 0.4380$, as detailed in the Supplemental Material [58] (see also the references [63–68] therein).

To ensure smoothness of $F_x^{\text{SORFKL}}(s, \beta = 0)$ between $s = 0$ and $s = s_0$, we further demand

$$F_x^{\text{SORFKL}}(s, \beta = 0) \geq F_x^{\text{Hyd}}(s_0) \text{ for } 0 \leq s \leq s_0. \quad (12)$$

Using Eqs. (9)–(12) and the exact exchange energy of H as constraints, we determine the coefficients $\{a_{ij}\}$ and $\{b_{ij}\}$ by fitting to the following appropriate norms: the exchange energies of rare-gas atoms and jellium surfaces [20]. In addition, we use the exact exchange HG energy density of H, the sole input directly utilized at the energy density level, to ensure gauge alignment. The final parameters, reference energies, and details on the optimization are summarized in the Supplemental Material [58] (see also the references [69, 70], [12, 67, 71], [20, 53, 72–78] therein).

The resulting F_x^{SORFKL} is smooth and fulfills the conditions specified by Eqs. (9)–(12) (see Fig. S2 of the Supplemental Material [58]). Due to condition (12), $F_x^{\text{SORFKL}}(s_0, \beta = 0) > F_x^{\text{Hyd}}(s_0)$. Although this sacrifices some gauge accuracy around nuclei, where $F_x^{\text{exact}} \approx F_x^{\text{Hyd}}(s_0)$, we prioritize smoothness here, as the latter is an important design criterion for numerical stability [24, 79].

The six exact constraints suitable for semilocal exchange DFAs are [20, 80]: (1) negativity, (2) spin-scaling, (3) uniform density scaling, (4) the gradient expansion for slowly varying electron densities, (5) non-uniform density scaling, and (6) the tight bound for single-orbital densities. In HG, we must sacrifice the constraints (5) and (6) that require $\lim_{s \rightarrow \infty} F_x(s, \beta) \sim s^{-1/2}$ and $F_x(s, \beta = 0) \leq 1.174$, respectively. These requirements contradict the asymptotic behavior of the exact exchange HG energy density, $\lim_{s \rightarrow \infty} F_x(s, \beta) \sim s/\ln(s)$. Constraints (5) and (6) are, together with the gradient expansion discussed next, the reason for SCAN’s significant deviation from the HG.

In HG, the gradient expansion of the exchange *energy density* for slowly varying densities is not well-defined due to an oscillatory term involving the Laplacian of the electron density that is not integrable [65, 81]. This non-integrable term can be removed via integration by parts, transforming the dependence on the Laplacian of the density into a dependence on the (reduced) density gradient [64, 65]. Although this procedure yields a well-defined gradient expansion for the exchange energy, the resulting exchange energy density is no longer in the HG [51]. For a semilocal DFA, it is inherently impossible to match the nonlocal nature of the exact exchange HG energy density for slowly varying densities. However, given the importance of the slowly varying density limit for solids [11, 20], SORFKL is designed to satisfy the second-order gradient expansion of the exchange *energy*.

TABLE I. Mean absolute percentage errors (MAPE) for exchange energies of rare-gas atoms and jellium surfaces (see the Supplemental Material [58] for detailed values, see also the references [12, 67, 71] therein).

	LDA	PBEsol	PBE	B88	SCAN	SORFKL
Rare-gas atoms	6.75	3.02	0.48	0.12	0.29	0.32
Jellium surfaces	45.5	2.75	21.1	28.8	24.5	0.62

Table I demonstrates that SORFKL achieves outstanding accuracy for both rare-gas atoms and jellium surfaces, ranking among the best in each category. For comparison, B88, designed to recover the correct asymptotic behavior of the exchange energy density and fitted to rare-gas exchange energies, achieves exceptional accuracy for rare-gas atoms but underperforms for jellium surfaces. In contrast, PBEsol, a revised version of PBE that was optimized for solids and recovering the first-principles second-order gradient expansion coefficient [11], achieves significantly improved accuracy for jellium surfaces, but at the cost of larger errors for rare-gas atoms. This reflects the trade-offs in functional design for finite and extended systems at the GGA level. Overall, SORFKL achieves accuracy for rare-gas atoms similar to the SCAN mGGA, but is by far the most accurate for jellium sur-

faces, even surpassing PBEsol.

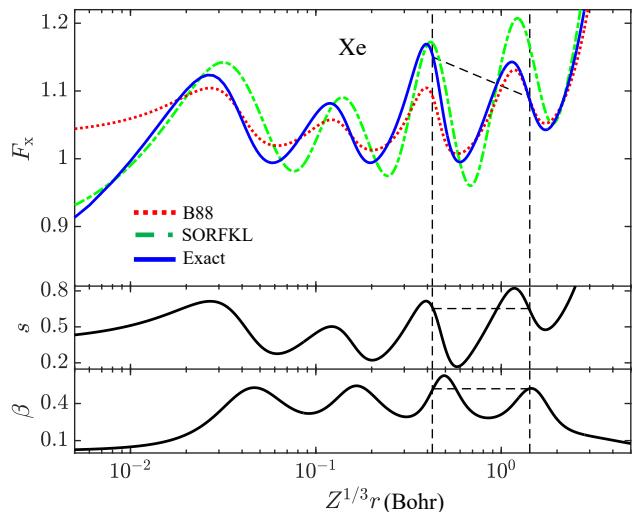


FIG. 2. Exchange enhancement factors of B88, SORFKL, and HG exact exchange, as well as s and β against $(Z^{1/3}r)$ for the xenon atom. Z is the nuclear charge.

Figure 2 compares the enhancement factors F_x of B88, SORFKL, and the exact exchange in HG as a function of $(Z^{1/3}r)$ for the xenon atom. Both B88 and SORFKL closely match F_x^{exact} in the tail region due to their recovery of the correct asymptotic behavior. Although B88 is highly accurate for the exchange energies of rare-gas atoms, it overestimates F_x^{exact} in the core region and in the shell regions where s is small. To compensate for this, B88 underestimates F_x^{exact} in the intershell regions where s is larger, resulting in damped oscillations compared to F_x^{exact} . SORFKL, on the other hand, achieves similar accuracy for the exchange energies but improves over B88 especially in the core region ($r = 0$). As a result, SORFKL aligns more closely with the exact exchange HG enhancement factor throughout all spatial regions.

Despite these achievements, we should point out that it is impossible to reproduce F_x^{exact} exactly over the entire spatial range with a semilocal DFA. For example, the vertical dashed lines in Fig. 2 correspond to two radial points with identical (s, β) values but different F_x^{exact} of approximately 1.15 and 1.09, respectively. Such behavior is impossible to capture with any semilocal DFA.

Next, we assess SORFKL across a diverse set of molecules, each representing a distinct chemical bonding environment: CH_4 for covalent bonding, Na_2 for metal-metal bonding, NaCl for ionic bonding, Ar_2 for van der Waals interactions, and $(\text{H}_2\text{O})_2$ for hydrogen bonding.

Figure 3 once again highlights that SCAN is in a gauge very different from HG, as it exhibits significant deviations from the exact exchange HG enhancement factor F_x^{exact} . Similarly to its performance on rare-gas atoms, B88 closely matches F_x^{exact} in the tail regions, but overes-

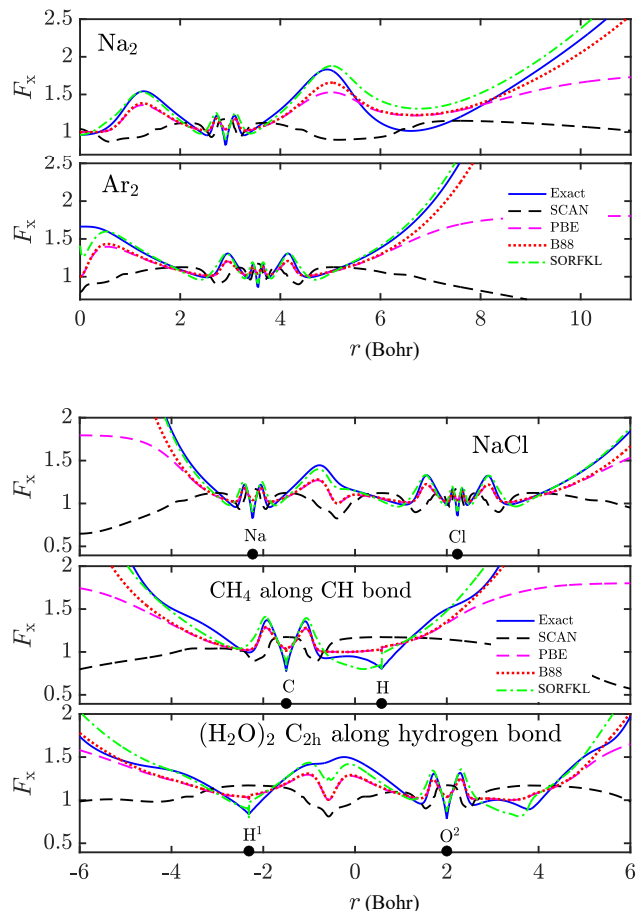


FIG. 3. Exchange enhancement factors F_x of selected DFAs and HG exact exchange along the bond axis of molecules representative of different chemical bond types. For Na_2 and Ar_2 , the bond center is at $r = 0$.

estimates F_x^{exact} in the core and shell regions and underestimates F_x^{exact} in the intershell regions. Interestingly, for the bonding regions of the considered molecules, B88 generally underestimates F_x^{exact} , except for the C–H bonds in CH_4 . PBE closely follows B88, except for the tail regions, where PBE does not recover the asymptotic behavior of the exact exchange HG energy density.

SORFKL outperforms B88 and PBE overall, achieving superior accuracy in the core, shell, intershell, and tail regions. Remarkably, SORFKL also closely tracks F_x^{exact} in the bonding regions, marking a significant improvement over B88. These results indicate that SORFKL accurately captures the exact exchange HG energy density for systems in equilibrium, where the exchange holes are localized.

In conclusion, we developed SORFKL, the first mGGA exchange functional explicitly constructed in HG. SORFKL restores the exact exchange HG energy density for both the uniform electron gas (UEG) and hydrogen, accurately capturing the asymptotic and core regions in

molecules and solids. Following SCAN’s design strategy, it satisfies all exact exchange constraints compatible with HG and uses appropriate norms. Beyond its immediate performance, SORFKL introduces a new paradigm for nonempirical functional development by leveraging gauge alignment as a core principle, enabling more consistent nonlocal corrections and unlocking the potential of large reference XC energy density datasets for machine learning. This foundation positions SORFKL as a promising step toward next-generation density functionals that combine exact constraint satisfaction, gauge consistency, and data-driven design, with potential as a general-purpose mGGA when paired with a suitable correlation functional.

ACKNOWLEDGMENTS

This work acknowledges the support of the U.S. DOE, Office of Science, Basic Energy Sciences Grant No. DE-SC0019350. This work also used Purdue Anvil CPU at Rosen Center for Advanced Computing (RCAC) through allocation DMR190076 from the Advanced Cyberinfrastructure Coordination Ecosystem: Services & Support (ACCESS) program, which is supported by National Science Foundation grants #2138259, #2138286, #2138307, #2137603, and #2138296. We thank John Perdew for discussions.

* These authors contributed equally to this work

† Corresponding Author: jsun@tulane.edu

- [1] P. Hohenberg and W. Kohn, *Physical Review* **136**, B864 (1964).
- [2] W. Kohn and L. J. Sham, *Physical Review* **140**, A1133 (1965).
- [3] K. Burke, *The Journal of Chemical Physics* **136** (2012).
- [4] A. D. Becke, *The Journal of Chemical Physics* **140** (2014).
- [5] H. S. Yu, S. L. Li, and D. G. Truhlar, *The Journal of Chemical Physics* **145** (2016).
- [6] N. Mardirossian and M. Head-Gordon, *Molecular Physics* **115**, 2315 (2017).
- [7] Y. Zhang, A. Ramasamy, K. Pokharel, M. Kothakonda, B. Xiao, J. W. Furness, J. Ning, R. Zhang, and J. Sun, *Wiley Interdisciplinary Reviews: Computational Molecular Science* **15**, e70007 (2025).
- [8] O. Gunnarsson and B. I. Lundqvist, *Physical Review B* **13**, 4274 (1976).
- [9] J. P. Perdew and Y. Wang, *Physical Review B* **45**, 13244 (1992).
- [10] J. P. Perdew, K. Burke, and M. Ernzerhof, *Physical Review Letters* **77**, 3865 (1996).
- [11] J. P. Perdew, A. Ruzsinszky, G. I. Csonka, O. A. Vydrov, G. E. Scuseria, L. A. Constantin, X. Zhou, and K. Burke, *Physical Review Letters* **100**, 136406 (2008).
- [12] A. D. Becke, *Physical Review A* **38**, 3098 (1988).

- [13] C. Lee, W. Yang, and R. G. Parr, *Physical Review B* **37**, 785 (1988).
- [14] A. D. Becke and M. R. Roussel, *Physical Review A* **39**, 3761 (1989).
- [15] J. Tao, J. P. Perdew, V. N. Staroverov, and G. E. Scuseria, *Physical Review Letters* **91**, 146401 (2003).
- [16] Y. Zhao and D. G. Truhlar, *The Journal of Chemical Physics* **125** (2006).
- [17] A. Ramasamy, L. Hou, J. V. Bazantes, T. J. Irons, A. M. Wibowo-Teale, T. Lebeda, and J. Sun, *Physical Review B* **112**, L161112 (2025).
- [18] J. Sun, B. Xiao, and A. Ruzsinszky, *The Journal of Chemical Physics* **137** (2012).
- [19] J. M. del Campo, J. L. Gázquez, S. Trickey, and A. Vela, *Chemical Physics Letters* **543**, 179 (2012).
- [20] J. Sun, A. Ruzsinszky, and J. P. Perdew, *Physical Review Letters* **115**, 036402 (2015).
- [21] N. Mardirossian and M. Head-Gordon, *The Journal of Chemical Physics* **142** (2015).
- [22] J. Tao and Y. Mo, *Physical Review Letters* **117**, 073001 (2016).
- [23] D. Mejia-Rodriguez and S. Trickey, *Physical Review A* **96**, 052512 (2017).
- [24] J. W. Furness, A. D. Kaplan, J. Ning, J. P. Perdew, and J. Sun, *The Journal of Physical Chemistry Letters* **11**, 8208 (2020).
- [25] T. Lebeda, T. Aschebrock, and S. Kümmel, *Physical Review Letters* **133**, 136402 (2024).
- [26] A. D. Becke, *The Journal of Chemical Physics* **98**, 1372 (1993).
- [27] A. D. Becke, *J. Chem. Phys.* **98**, 5648 (1993).
- [28] J. P. Perdew, M. Ernzerhof, and K. Burke, *The Journal of Chemical Physics* **105**, 9982 (1996).
- [29] J. Heyd, G. E. Scuseria, and M. Ernzerhof, *The Journal of Chemical Physics* **118**, 8207 (2003).
- [30] X. Xu and W. A. Goddard III, *Proceedings of the National Academy of Sciences* **101**, 2673 (2004).
- [31] Y. Zhao and D. G. Truhlar, *Theoretical Chemistry Accounts* **120**, 215 (2008).
- [32] G. I. Csonka, J. P. Perdew, and A. Ruzsinszky, *Journal of Chemical Theory and Computation* **6**, 3688 (2010).
- [33] N. Mardirossian and M. Head-Gordon, *The Journal of Chemical Physics* **144** (2016).
- [34] D. C. Langreth and J. P. Perdew, *Solid State Communications* **17**, 1425 (1975).
- [35] J. Kirkpatrick, B. McMorrow, D. H. Turban, A. L. Gaunt, J. S. Spencer, A. G. Matthews, A. Obika, L. Thiry, M. Fortunato, D. Pfau, *et al.*, *Science* **374**, 1385 (2021).
- [36] J. P. Perdew, V. N. Staroverov, J. Tao, and G. E. Scuseria, *Physical Review A—Atomic, Molecular, and Optical Physics* **78**, 052513 (2008).
- [37] M. Haasler, T. M. Maier, R. Grotjahn, S. Guckel, A. V. Arbuznikov, and M. Kaupp, *Journal of Chemical Theory and Computation* **16**, 5645 (2020).
- [38] J. P. Perdew and A. Zunger, *Physical Review B* **23**, 5048 (1981).
- [39] M. R. Pederson, A. Ruzsinszky, and J. P. Perdew, *The Journal of Chemical Physics* **140**, 121103 (2014).
- [40] C. Li, X. Zheng, N. Q. Su, and W. Yang, *National Science Review* **5**, 203 (2018).
- [41] Y. Zhang, J. Furness, R. Zhang, Z. Wang, A. Zunger, and J. Sun, *Physical Review B* **102**, 045112 (2020).
- [42] A. D. Becke, *The Journal of Chemical Physics* **138**, 074109 (2013).
- [43] N. Q. Su, C. Li, and W. Yang, *Proceedings of the National Academy of Sciences* **115**, 9678 (2018).
- [44] E. R. Johnson and J. Contreras-García, *The Journal of Chemical Physics* **135** (2011).
- [45] J. P. Perdew, A. Ruzsinszky, J. Sun, N. K. Nepal, and A. D. Kaplan, *Proceedings of the National Academy of Sciences* **118**, e2017850118 (2021).
- [46] R. J. McCarty, D. Perchak, R. Pederson, R. Evans, Y. Qiu, S. R. White, and K. Burke, *Physical Review Letters* **125**, 266401 (2020).
- [47] K. Burke, F. G. Cruz, and K.-C. Lam, *The Journal of Chemical Physics* **109**, 8161 (1998).
- [48] A. V. Arbuznikov and M. Kaupp, *The Journal of Chemical Physics* **141**, 204101 (2014).
- [49] A. V. Arbuznikov, A. Wodyński, and M. Kaupp, *The Journal of Chemical Physics* **161**, 164104 (2024).
- [50] R. R. Zope, Y. Yamamoto, C. M. Diaz, T. Baruah, J. E. Peralta, K. A. Jackson, B. Santra, and J. P. Perdew, *The Journal of Chemical Physics* **151** (2019).
- [51] P. Bhattarai, K. Wagle, C. Shahi, Y. Yamamoto, S. Romero, B. Santra, R. R. Zope, J. E. Peralta, K. A. Jackson, and J. P. Perdew, *The Journal of Chemical Physics* **152**, 214109 (2020).
- [52] J. P. Perdew, K. Burke, and Y. Wang, *Physical Review B* **54**, 16533 (1996).
- [53] J. Tao, V. N. Staroverov, G. E. Scuseria, and J. P. Perdew, *Physical Review A—Atomic, Molecular, and Optical Physics* **77**, 012509 (2008).
- [54] G. Oliver and J. Perdew, *Physical Review A* **20**, 397 (1979).
- [55] J. Sun, B. Xiao, Y. Fang, R. Haunschild, P. Hao, A. Ruzsinszky, G. I. Csonka, G. E. Scuseria, and J. P. Perdew, *Physical Review Letters* **111**, 106401 (2013).
- [56] J. W. Furness and J. Sun, *Physical Review B* **99**, 041119 (2019).
- [57] T. Lebeda and S. Kümmel, *Phys. Rev. B* **111**, 155133 (2025).
- [58] See the Supplemental Material at [URL will be inserted by publisher] for plots of $g(s, \beta)$ and $F_x(s, \beta)$ as functions of s for different DFAs including SORFKL, the derivation of $F_x^{\text{Hyd}}(s)$, the second-order gradient expansion of F_x^{SORFKL} , computational details and optimal parameters, exchange energies of rare-gas atoms and jellium surface energies for different r_s values across DFAs, as well as F_x of additional rare-gas atoms as a function of r , and F_x and binding energies of H_2^+ for different DFAs.
- [59] C.-O. Almbladh and U. von Barth, *Physical Review B* **31**, 3231 (1985).
- [60] N. March, *Physical Review A* **36**, 5077 (1987).
- [61] T. Aschebrock and S. Kümmel, *Phys. Rev. Res.* **1**, 033082 (2019).
- [62] O. A. Vydrov and T. Van Voorhis, *Physical Review Letters* **103**, 063004 (2009).
- [63] P. Antoniewicz and L. Kleinman, *Physical Review B* **31**, 6779 (1985).
- [64] J. P. Perdew, *Physical Review Letters* **55**, 1665 (1985).
- [65] E. Gross and R. Dreizler, *Zeitschrift für Physik A Atoms and Nuclei* **302**, 103 (1981).
- [66] M. Brack, B. Jennings, and Y. Chu, *Physics Letters B* **65**, 1 (1976).
- [67] J. W. Furness, A. D. Kaplan, J. Ning, J. P. Perdew, and J. Sun, *The Journal of Chemical Physics* **156**, 034109

- (2022).
- [68] J. Sun, J. P. Perdew, and A. Ruzsinszky, Proceedings of the National Academy of Sciences **112**, 685 (2015).
- [69] K. V. Price, R. M. Storn, and J. A. Lampinen, Differential evolution: a practical approach to global optimization, 37 (2005).
- [70] P. Virtanen, R. Gommers, T. E. Oliphant, M. Haberland, T. Reddy, D. Cournapeau, E. Burovski, P. Peterson, W. Weckesser, J. Bright, *et al.*, Nature methods **17**, 261 (2020).
- [71] J. Pitarke and A. Eguiluz, Physical Review B **63**, 045116 (2001).
- [72] E. Clementi and C. Roetti, Atomic data and nuclear data tables **14**, 177 (1974).
- [73] J. Furness and S. Lehtola, code repository available at <https://github.com/JFurness1/AtomicOrbitals> (2021).
- [74] F. Jorge and M. Franco, Chemical Physics **253**, 21 (2000).
- [75] D. G. Smith, L. A. Burns, A. C. Simmonett, R. M. Parrish, M. C. Schieber, R. Galvelis, P. Kraus, H. Kruse, R. Di Remigio, A. Alenaizan, *et al.*, The Journal of Chemical Physics **152** (2020).
- [76] E. W. Lemmon, M. L. Huber, M. O. McLinden, *et al.*, Reference fluid thermodynamic and transport properties (REFPROP), version **9** (2010).
- [77] T. H. Dunning Jr, The Journal of Chemical Physics **90**, 1007 (1989).
- [78] A. K. Wilson, T. Van Mourik, and T. H. Dunning Jr, Journal of Molecular Structure: THEOCHEM **388**, 339 (1996).
- [79] M. G. Medvedev, I. S. Bushmarinov, J. Sun, J. P. Perdew, and K. A. Lyssenko, Science **355**, 49 (2017); K. P. Kepp, Science **356**, 496 (2017); M. G. Medvedev, I. S. Bushmarinov, J. Sun, J. P. Perdew, and K. A. Lyssenko, Science **356**, 496 (2017).
- [80] A. D. Kaplan, M. Levy, and J. P. Perdew, Annu. Rev. Phys. Chem. **74**, 193 (2023).
- [81] R. Armiento and A. E. Mattsson, Physical Review B **66**, 165117 (2002).

Supplementary material for “Meta-generalized gradient approximation made in the Hartree gauge”

Yan Oueis,^{1,*} Akilan Ramasamy,^{1,*} James W. Furness,^{1, a)} Jamin Kidd,¹ Timo Lebeda,¹ and Jianwei Sun^{1, †}

¹*Department of Physics and Engineering Physics,
Tulane University, New Orleans, LA 70118, USA*

a) Current address: Schrödinger, Inc., New York City, New York 10036, USA

(Dated: March 13, 2026)

Here, we provide figures of $g(s, \beta)$ and $F_x(s, \beta)$, a derivation of F_x^{Hyd} and its asymptotic behavior, details on the second-order gradient expansion of F_x^{SORFKL} , on SORFKL’s parameters, and on the exchange energies of rare-gas atoms and jellium surfaces, and the computational details. Furthermore, we show enhancement factor plots for more rare-gas atoms and discuss the enhancement factor in the context of the H_2^+ binding energy curve.

REPLACING s WITH $g(s, \beta)$ AND A COMPARISON OF $F_x^{\text{SORFKL}}(s, \beta)$ WITH $F_x^{\text{Hyd}}(s)$, $F_x^{\text{B88}}(s)$, AND $F_x^{\text{PBE}}(s)$

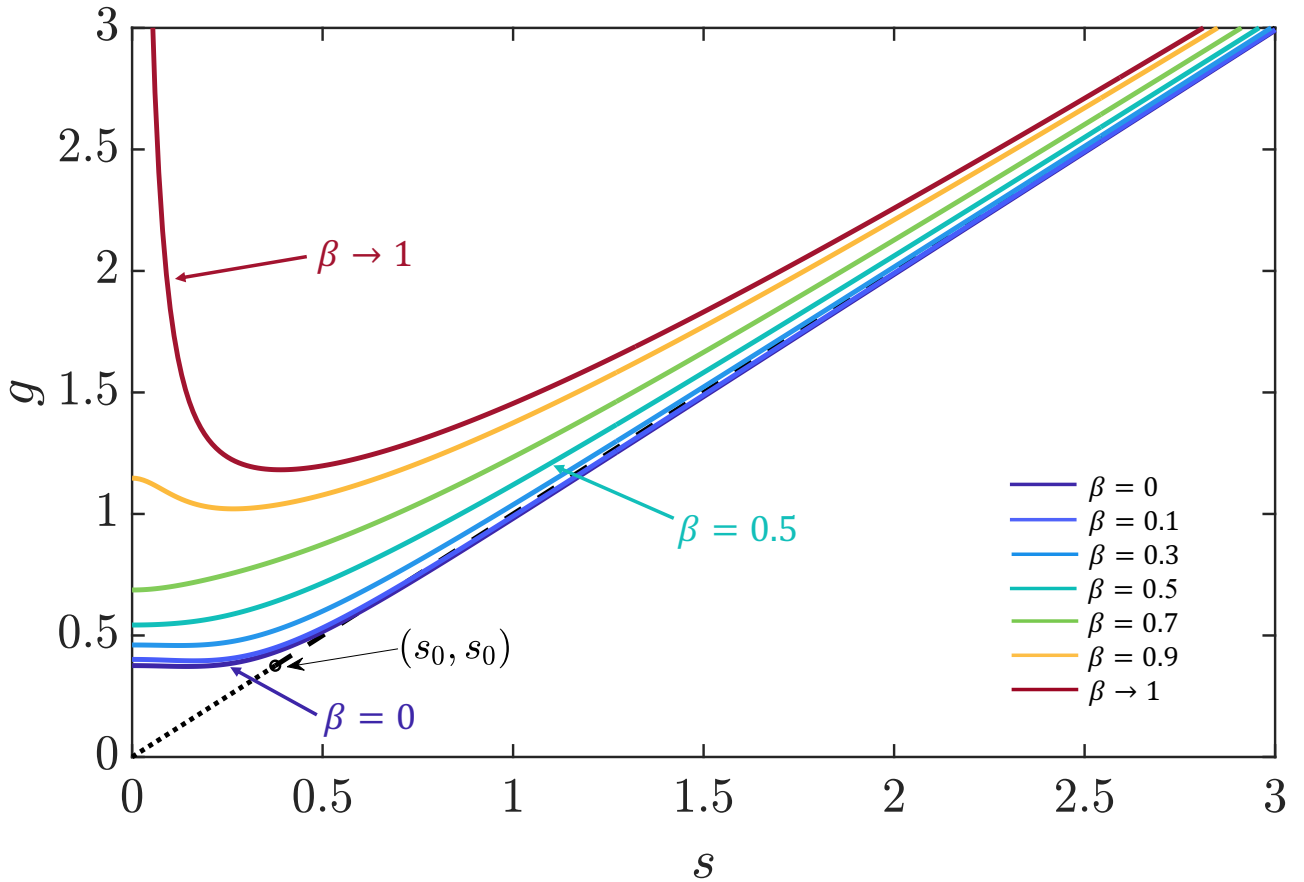


Figure S1. $g(s, \beta)$ is plotted against s at different β . The line $g = s$ is plotted with a dashed line for $s \geq s_0$ and with a dotted line for $s \leq s_0$, where $s_0 = (6\pi)^{-1/3}$ is the s value at the hydrogen nucleus.

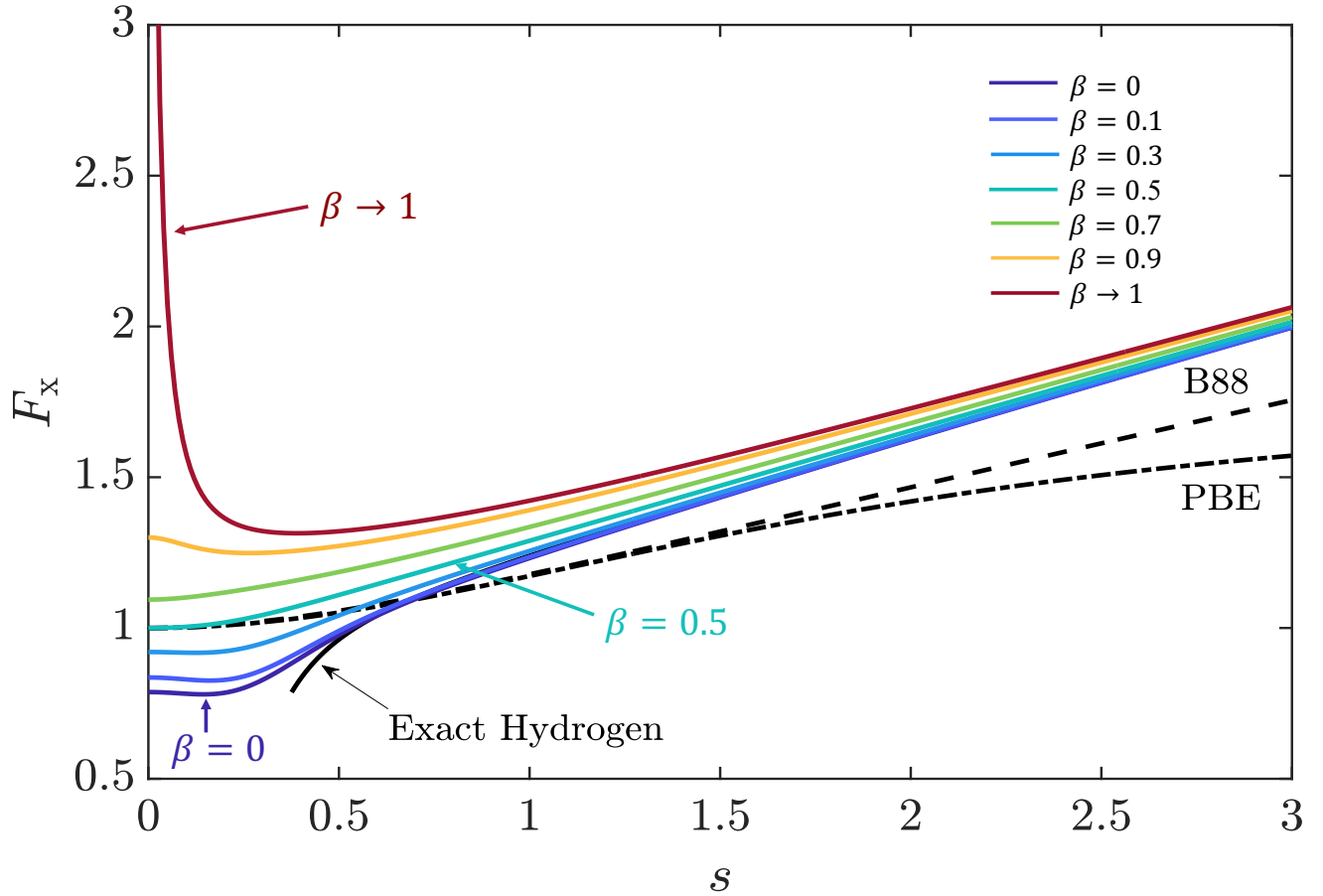


Figure S2. $F_x^{\text{SORFKL}}(s, \beta)$ as function of s for different β along with $F_x^{\text{Hyd}}(s)$ (solid), $F_x^{\text{B88}}(s)$ (dashed), and $F_x^{\text{PBE}}(s)$ (dot-dashed). $F_x^{\text{Hyd}}(s)$ is shown only for $s > s_0$ with $s_0 = (6\pi)^{-1/3}$.

DERIVATION OF $F_x^{\text{Hyd}}(s)$ AND ITS ASYMPTOTIC BEHAVIOR

The fully spin-polarized electron density of the hydrogen atom is

$$n^H(r) = \frac{e^{-2r}}{\pi}. \quad (\text{S1})$$

For one-electron systems, the correlation energy vanishes and the exchange energy equals the negative of the Hartree energy. Consequently, the exchange energy can be expressed as

$$E_x[n] = -\frac{1}{2} \int d^3r \int d^3r' \frac{n(\mathbf{r})n(\mathbf{r}')}{|\mathbf{r} - \mathbf{r}'|}, \quad (\text{S2})$$

and the exchange hole here is $n_x(\mathbf{r}, \mathbf{r}') = -n(\mathbf{r}')$. Therefore, the exchange energy density per electron in the Hartree gauge (HG) is (after integrating over the spherical degrees of freedom)

$$\varepsilon_x(r) = -\frac{1}{2} \left[\int_0^r dr' \frac{4\pi r'^2 n(r')}{r} + \int_r^\infty 4\pi r' n(r') \right]. \quad (\text{S3})$$

Inserting the hydrogen electron density, Eq. (S1), the exact exchange HG energy density per electron of H reads

$$\varepsilon_x^{\text{exact}}(r) = -\frac{1}{2r} \left(1 - e^{-2r}(1+r) \right), \quad (\text{S4})$$

Thus,

$$\begin{aligned} F_x^{exact}(r) &= \frac{\varepsilon_x^{exact}(r)}{\varepsilon_x^{uni}(r)} \\ &= 2 \left(\frac{\pi}{9} \right)^{2/3} \frac{e^{-\frac{4r}{3}}}{r} \left[e^{2r} - r - 1 \right], \end{aligned} \quad (S5)$$

where $\varepsilon_x^{uni}(n) = -3/(4\pi)(3\pi^2 n)^{1/3}$. Obviously, Eq. (S4) leads to $\lim_{r \rightarrow \infty} \varepsilon_x^{exact}(r) = -\frac{1}{2r}$.

The $F_x^{Hyd}(s)$ model is defined for spin-unpolarized systems. Therefore, after applying the spin scaling relationship, the exchange energy of the hydrogen atom calculated with the $F_x^{Hyd}(s)$ model is

$$E_x^{Hyd}[n^H, 0] = \frac{1}{2} \int d^3r e_x^{uni}(2n^H) F_x^{Hyd}(s[2n^H]). \quad (S6)$$

By requiring the exchange energy density of Eq. (S6) reproducing the exact exchange HG energy density, we have,

$$F_x^{exact}(r) = 2^{1/3} F_x^{Hyd}(s[2n^H]). \quad (S7)$$

From the definition of s , we have

$$s[2n^H] = \frac{e^{\frac{2r}{3}}}{(6\pi)^{\frac{1}{3}}}. \quad (S8)$$

By combining Eqs. (S5) and (S7), replacing r with s , and rearranging terms, we arrive at Eq. (4) of the main text.

For a finite system, the electron density at the asymptotic region decays exponentially as,

$$\lim_{r \rightarrow \infty} n(\mathbf{r}) = e^{-\delta r}, \quad (S9)$$

where $n^H(r)$ follows the same form. Here, δ is a constant related to the ionization potential of the system [1]. The corresponding reduced density gradient there diverges as $\lim_{r \rightarrow \infty} s = \frac{\delta e^{\delta r/3}}{2(3\pi^2)^{1/3}}$. Since $\lim_{s \rightarrow \infty} F_x^{Hyd}(s) = \frac{4\pi}{9} \frac{s}{\ln(s)}$, any enhancement factor F_x^{mGGA} recovering $\lim_{s \rightarrow \infty} F_x^{Hyd}(s)$ leads to $\lim_{r \rightarrow \infty} \varepsilon_x^{mGGA}(r) = -\frac{1}{2r}$, which is the exact asymptotic behavior of the exchange energy density per electron of the finite system in the Hartree gauge [2]. These have been carefully discussed in Ref. [3].

THE SECOND-ORDER GRADIENT EXPANSION OF $F_x^{SORFKL}(s, \beta)$

The second-order gradient expansion for the exchange energy of a slowly varying electron density can be satisfied by requiring [4-6]

$$\lim_{|\nabla n| \rightarrow 0} F_x^{SORFKL}(s, \beta) = 1 + \frac{10}{81} s^2. \quad (S10)$$

Using the gradient expansion of τ [7],

$$\tau = \tau^{uni} \left[1 + \frac{20}{9} q + \frac{5}{27} s^2 \right] + \mathcal{O}[|\nabla n|^4], \quad (S11)$$

where $q = \nabla^2 n / [4(3\pi^2)^{2/3} n^{5/3}]$ is the reduced electron density Laplacian, we have

$$\lim_{|\nabla n| \rightarrow 0} (1 - 2\beta) = -\frac{10}{9} q + \frac{85}{54} s^2 + \mathcal{O}[|\nabla n|^4]. \quad (S12)$$

Under integration by parts [8, 9], q can be recast in terms of s^2 , leading to

$$q \stackrel{p.I.}{\cong} s^2/3. \quad (S13)$$

The second order gradient expansion of $g(s, \beta)$ then reads

$$\lim_{|\nabla n| \rightarrow 0} g(s, \beta) = \left(\frac{a_{00}}{b_{00}} \right)^{\frac{1}{2}} (1 + \Delta g^{(2)}(s)) , \quad (\text{S14})$$

with

$$\Delta g^{(2)}(s) = \left[\frac{65}{108} \left(\frac{a_{01}}{a_{00}} - \frac{b_{01}}{b_{00}} \right) + \frac{1}{2} \left(\frac{a_{10}}{a_{00}} - \frac{a_2}{b_{00}} \right) \right] s^2 . \quad (\text{S15})$$

Thus,

$$\lim_{|\nabla n| \rightarrow 0} F_x^{\text{SORFKL}}(s, \beta) = C_1 + C_2 \Delta g^{(2)}(s) , \quad (\text{S16})$$

where

$$C_1 = \frac{1}{9} \left[\frac{\frac{2}{3} \left(6\pi \sqrt{\frac{a_{00}}{b_{00}} - \frac{b_{00}}{a_{00}}} \right)}{\left(\frac{1}{3} \right) \ln(6\pi) + \frac{1}{2} \ln \left(\frac{a_{00}}{b_{00}} \right)} - \frac{b_{00}}{a_{00}} \right] , \quad (\text{S17})$$

and

$$C_2 = \frac{2}{27} \left[\frac{6\pi \sqrt{\frac{a_{00}}{b_{00}} + \frac{2b_{00}}{a_{00}}}}{\ln(6\pi)^{1/3} + \frac{1}{2} \ln \frac{a_{00}}{b_{00}}} - \frac{6\pi \sqrt{\frac{a_{00}}{b_{00}} - \frac{b_{00}}{a_{00}}}}{\left(\ln(6\pi)^{1/3} + \frac{1}{2} \ln \frac{a_{00}}{b_{00}} \right)^2} \right] + \frac{2}{9} \frac{b_{00}}{a_{00}} . \quad (\text{S18})$$

To recover the second order gradient expansion, we require $C_1 = 1$, leading to

$$\frac{a_{00}}{b_{00}} \approx 0.29480 , \quad (\text{S19})$$

(note that we set $b_{00} = 1$ without loss of generality and thus $a_{00} \approx 0.2948$) and $C_2 \Delta g^{(2)}(s) = \frac{10}{81} s^2$, leading to

$$\frac{a_2}{b_{00}} = \frac{a_{10}}{a_{00}} - \frac{20}{81 C_2} - \frac{65}{54} \left(\frac{b_{01}}{b_{00}} - \frac{a_{01}}{a_{00}} \right) , \quad (\text{S20})$$

which relates a_{10} , a_{01} , a_2 , and b_{01} .

SORFKL'S PARAMETERS

Table S1 summarizes the parameters of SORFKL. For the optimization of SORFKL's parameters, we used the differential evolution algorithm [10] as implemented in SciPy.Optimize library version 1.11.1 [11].

Table S1. Values of parameters for $F_x^{\text{SORFKL}}(s, \beta)$.

a_{00}	a_{01}	a_{02}	a_{10}	a_{11}
0.2948	0	-0.0253	3.9226	-5.6680
a_{12}	b_{00}	b_{01}	b_{02}	a_2
2.8873	1	0.9545	-0.0455	11.5935

The total loss function was constructed as a weighted sum of scaled loss functions for the exchange energies of the rare-gas atoms, the jellium surface exchange energies, and the exact exchange HG energy density of the hydrogen atom (the latter as measure of hydrogen atom gauge accuracy).

The scaled loss functions were computed using the following general equation:

$$\tilde{\mathcal{L}} = \frac{\mathcal{L}}{\epsilon_{\max}} , \quad (\text{S21})$$

where \mathcal{L} and ϵ_{\max} are the loss functions and the maximum reference errors respectively. For the rare-gas atoms, \mathcal{L} is the MAPE in E_x for Ne, Ar, Kr, and Xe, and ϵ_{\max} is PBEsol’s MAPE for the same atoms. For the jellium surface loss function, \mathcal{L} is the MAPE in jellium surface exchange energies σ_x for $r_s = 2$, $r_s = 3$, $r_s = 4$, and $r_s = 6$, and ϵ_{\max} is PBE’s MAPE in σ_x for the same bulk constants.

The hydrogen atom gauge loss is defined as,

$$\mathcal{L}^{Hyd} = \sum_{r_i=r_{min}}^{r_{max}} |e_x^{exact}(r_i) - e_x^{SORFKL}(r_i)|^2, \quad (S22)$$

where the sum is computed over 1000 discrete radial points, ranging from $r_{\min} = 0.01$ Bohr to $r_{\max} = 10$ Bohr, covering both the near-nucleus and asymptotic regions. The analytic electron density of hydrogen atom is used here. For the scaled $\tilde{\mathcal{L}}^{Hyd}$, ϵ_{\max} is set to 5×10^{-3} , which is arbitrary but a reasonably small number for the optimization.

Using the above definitions, the total loss functions can be written as:

$$\tilde{\mathcal{L}}^{Total} = \omega_1 \tilde{\mathcal{L}}^{rare-gas} + \omega_2 \tilde{\mathcal{L}}^{Jellium} + \omega_3 \tilde{\mathcal{L}}^{Hyd}, \quad (S23)$$

with hyperparameters ω_i responsible for relative contribution of individual scaled loss functions. Results presented in this paper correspond to $\omega_1 = 0.75$, $\omega_2 = 0.05$, and $\omega_3 = 0.2$. We observed, however, that the results of the optimization are not markedly affected by the values assigned to ω_i ’s as long as the relative contributions from the rare-gas atoms and jellium surfaces stay above 70% and below 10%, respectively.

COMPUTATIONAL DETAILS

The exchange energies of different density functionals and the exchange enhancement factor plots for rare-gas atoms were calculated from HF reference datasets with Slater-type orbitals [12, 13], with the reference HF exchange energies from Ref. [3]. For the jellium surfaces, LDA orbitals were used [14].

Following Ref. [15], the Universal Gaussian Basis Set (UGBS) [16] was used for calculating the enhancement factors of molecules shown in Figure 4 of the main text and for Figure S4. The corresponding calculations were carried out in Psi4 [17]. HF calculations provided density matrices that were used to derive HF electron densities and kinetic energy densities. These densities were then used to compute exchange enhancement factors of various functionals. Experimental molecular geometries were sourced from the NIST database [18] and used without further optimization.

The binding energy curves of H_2^+ were obtained using Psi4 with the cc-pV5Z basis set [19, 20]. The HF density was used in a non-self-consistent manner to evaluate the exchange energies for the considered density functionals. The binding energy curves for H_2^+ were generated based solely on the exchange functional, excluding the correlation functional contributions (which would be non-vanishing for the PBE GGA).

EXCHANGE ENERGIES OF RARE-GAS ATOMS AND JELLIUM SURFACE FOR DIFFERENT r_s

Tables S2 and S3 report the detailed data for the exchange energies of rare-gas atoms and jellium surfaces that supplement Table I of the main text.

Table S2. Exchange energies (Ha) of rare-gas atoms and the corresponding mean absolute percentage errors (MAPE) of the SORFKL and other functionals.

	Ne	Ar	Kr	Xe	MAPE (%)
Exact ^a	-12.108	-30.188	-93.89	-179.2	-
LDA	-11.033	-27.863	-88.62	-170.6	6.75
PBEsol	-11.665	-29.143	-91.45	-175.0	3.02
PBE	-12.067	-29.996	-93.43	-178.4	0.48
B88	-12.138	-30.153	-93.87	-179.0	0.12
SCAN ^b	-12.164	-30.264	-94.071	-179.315	0.29
SORFKL	-12.203	-30.204	-93.774	-178.639	0.32

^a From [3]

^b From [8]

Table S3. Relative signed errors of the SORFKL and other functionals for the jellium surface exchange energies σ_x (erg/cm²) at various bulk density parameters r_s . The relative signed error is defined as $\frac{\sigma_x^{DFA} - \sigma_x^{exact}}{\sigma_x^{exact}} * 100$

	$r_s = 2$	$r_s = 3$	$r_s = 4$	$r_s = 6$	MAPE (%)
Exact ^a	2624	526	157	22	–
LDA	15.72	27.15	41.78	97.27	45.5
PBEsol	1.589	2.627	3.295	3.478	2.75
PBE	–7.150	–11.73	–18.45	–47.08	21.1
B88	–9.364	–15.71	–25.05	–64.93	28.8
SCAN ^b	0.27	–7.02	–19.18	–71.53	24.5
SORFKL	–1.527	–0.760	–0.197	0.008	0.62

^a From [21]

^b From [8]

ENHANCEMENT FACTOR PLOTS FOR MORE RARE-GAS ATOMS

Figure S3 shows the exchange enhancement factors in rare-gas atoms and complements Fig. 2 of the main text.

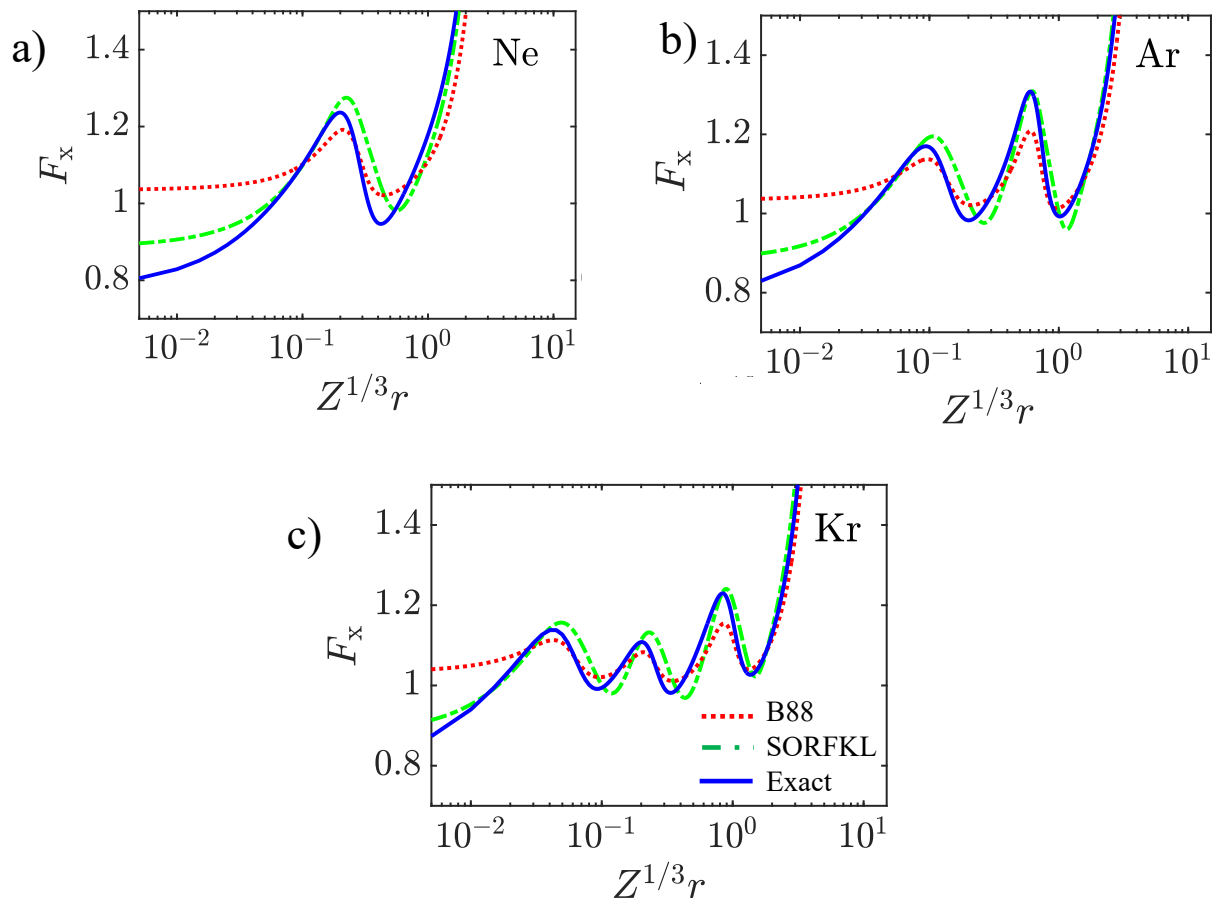


Figure S3. Exchange enhancement factors of B88, SORFKL, and exact exchange in HG against $Z^{1/3}r$ (in Bohr) for Ne, Ar and Kr. Z is the nuclear charge.

SORFKL's ability to recover the exact exchange HG energy density more closely than B88 stems from its mGGA nature. In particular, this allows SORFKL to recover the exact exchange HG energy density for both UEG and H, while maximally satisfying exact constraints. By incorporating the kinetic energy density via the dependence

on β , SORFKL can distinguish different chemical environments [22], allowing for the design of distinct exchange enhancement factors across these environments. For instance, $\beta = 0$ corresponds to single-orbital systems and regions such as H and core regions, while $\beta \approx 1/2$ characterizes slowly varying densities, enabling tailored GGA-like behavior for each regime [14], as shown in Fig. S2.

EXCHANGE ENHANCEMENT FACTORS AND BINDING ENERGY CURVES OF H_2^+

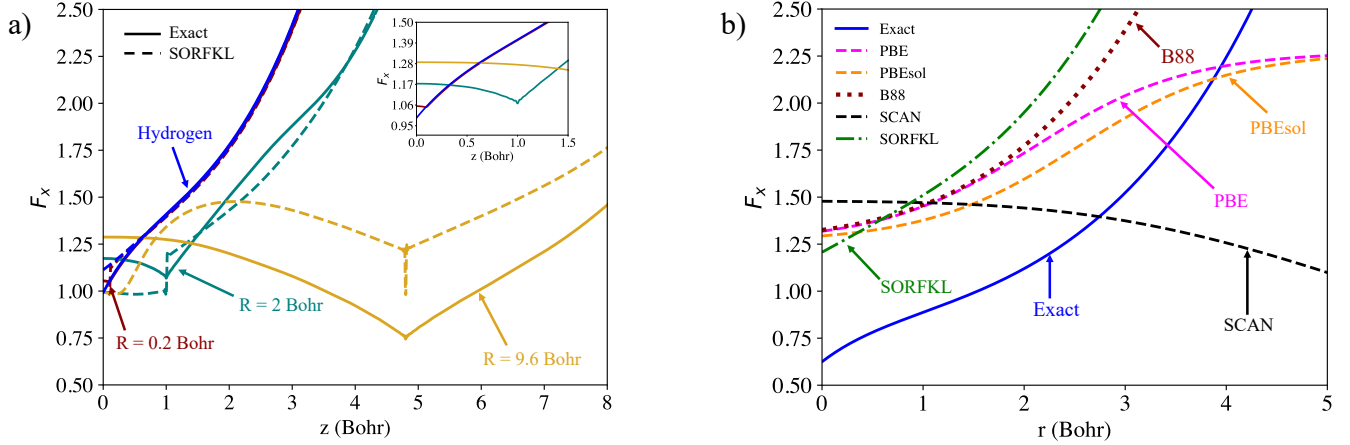


Figure S4. a) Exchange enhancement factors of exact exchange and SORFKL along the bond axis z of H_2^+ for various bond lengths R , using the UGBS basis set. Solid lines represent the exact exchange F_x , while dashed lines depict the F_x of SORFKL. The systems are centered at $z = 0$, with the nuclear positions of H_2^+ for a given bond length R indicated by the cusps in F_x at $z = R/2$. b) Enhancement factors of various DFAs compared with the exact exchange F_x for $H_2^+(R \rightarrow \infty)$. At $R \rightarrow \infty$, half of an electron remains bound to each proton, with the electron density $n^H(r)/2$ around each proton. Since the bond center has negligible influence on the electron density near the protons, the exchange enhancement factors are computed using $n^H(r)/2$ and plotted as a function of r , where $r = 0$ represents the proton position.

The H_2^+ molecular ion serves as a prototypical system for illustrating SIE, which arises from the incomplete cancellation of the spurious Coulomb interaction between an electron and itself. In H_2^+ , the exchange hole is highly localized as the bond length $R \rightarrow 0$ and becomes increasingly delocalized as R increases. In the limit $R \rightarrow 0$, the exact exchange HG enhancement factor F_x^{exact} becomes that of hydrogen, whereas for $R \rightarrow \infty$, it converges to F_x^{exact} of $n^H(r)/2$ centered at each of the two protons, where $n^H(r)$ is the electron density of an isolated hydrogen atom.

Figure S4 a) illustrates the evolution of F_x with R , showing that $F_x^{\text{exact}}(z = 0)$, the exact exchange HG enhancement factor at the bond center, decreases as R decreases and converges to $F_x^{\text{exact}}(r = 0)$ at the nucleus of an isolated hydrogen as $R \rightarrow 0^+$. In the limit $R \rightarrow 0^+$, $s = 0$ remains at the bond center due to symmetry, while the electron density reduces to the hydrogenic $1s$ orbital density of He^+ , yielding an exact exchange HG enhancement factor identical to that of the isolated hydrogen atom. This confirms that $F_x^{\text{exact}}(z = 0)$ of $H_2^+(R \rightarrow 0^+)$ equals that of the isolated hydrogen atom at its nucleus, justifying $F_x^{\text{SORFKL}}(s = 0, \beta = 0) = F_x^{\text{Hyd}}(s_0)$.

As R increases, $F_x^{\text{exact}}(z = 0)$ grows and eventually diverges ($F_x^{\text{exact}} \rightarrow \infty$ as $R \rightarrow \infty$), similarly to the two identical closed shell atoms discussed in the main text, and consistent with the expected asymptotic behavior of a finite system. Thus, for all R we have $\beta = 0$ and $s = 0$ at the bond center, but F/x^{exact} increases from $F_x^{\text{Hyd}}(s_0)$ for $R = 0^+$ to infinity as $R \rightarrow \infty$. This underlines again the limitation of the semilocal form in recovering the exact exchange HG energy density everywhere. However, since the bond center in the dissociation limit is a region of delocalized exchange hole, a semilocal DFA such as SORFKL is not expected to be accurate there. Consequently, SORFKL closely matches the exact exchange HG enhancement factor for small R , but the deviation increases with increasing R .

Figure S4 b) compares the enhancement factors of various DFAs with F_x^{exact} in HG for $H_2^+(R \rightarrow \infty)$. In this dissociation limit, the bond center has negligible influence on the electron density around the protons, and the electron density around each atomic center becomes $n^H(r)/2$. Consequently, the exact exchange HG enhancement factor around one nuclear center is given by $2^{-2/3}F_x^{\text{Hyd}}(r)$. For Figure S4 b), we thus calculate the exchange enhancement factors using $n^H(r)/2$ and plot them as a function of r , with $r = 0$ representing the proton position. Apparently, the SORFKL exchange enhancement factor is approximately $2^{2/3}$ times larger than that of the exact exchange in

HG, indicating that the underlying exchange hole of SORFKL is significantly deeper than the exact exchange hole for a reference electron at any spatial point, as expected. Similar behavior is observed for B88 with smaller F_x than that of SORFKL, while PBE and PBEsol cross the exact exchange curve for $r > 4$ Bohr. SCAN exhibits the strongest deviation from SORFKL and F_x^{exact} and crosses the exact exchange curve for $r > 3$ Bohr. Correspondingly, the exchange energies of $H_2^+(R \rightarrow \infty)$ are -0.4809 Ha (PBEsol), -0.5080 Ha (PBE), -0.5176 Ha (B88), -0.4940 Ha (SCAN), -0.5401 Ha (SORFKL), and -0.3125 Ha (Exact).

As shown in Figure S5, at and before the equilibrium bond length ($R = 1.058 \text{ \AA}$), the exchange energies of the semilocal DFAs align closely with the reference HF result. Interestingly, SORFKL provides the most accurate binding energy at equilibrium, outperforming all other DFAs considered, including SCAN. However, as the bond length increases and the exchange hole becomes more delocalized, all semilocal approximations yield increasingly negative binding energies, with SORFKL exhibiting the most pronounced deviation. This behavior is consistent with the semilocal DFA's performance in F_x and the associated exchange energies for $H_2^+(R \rightarrow \infty)$, as illustrated in Figure S4 b). These findings highlight the inherent limitations of semilocal density functionals in accurately describing H_2^+ with stretched bonds, underscoring the necessity of incorporating nonlocal corrections into the functional form [23, 24].

We emphasize once more that mGGAs are semilocal DFAs and thus not appropriate for modeling systems with delocalized exchange holes, where semilocal DFAs typically exhibit too negative exchange energies. Therefore, in the same gauge, semilocal density functionals are in general expected to have larger enhancement factors than the exact exchange for systems with delocalized exchange holes. This is what we observe for SORFKL in Figure S4 a) for $R = 9.6$ Bohr.

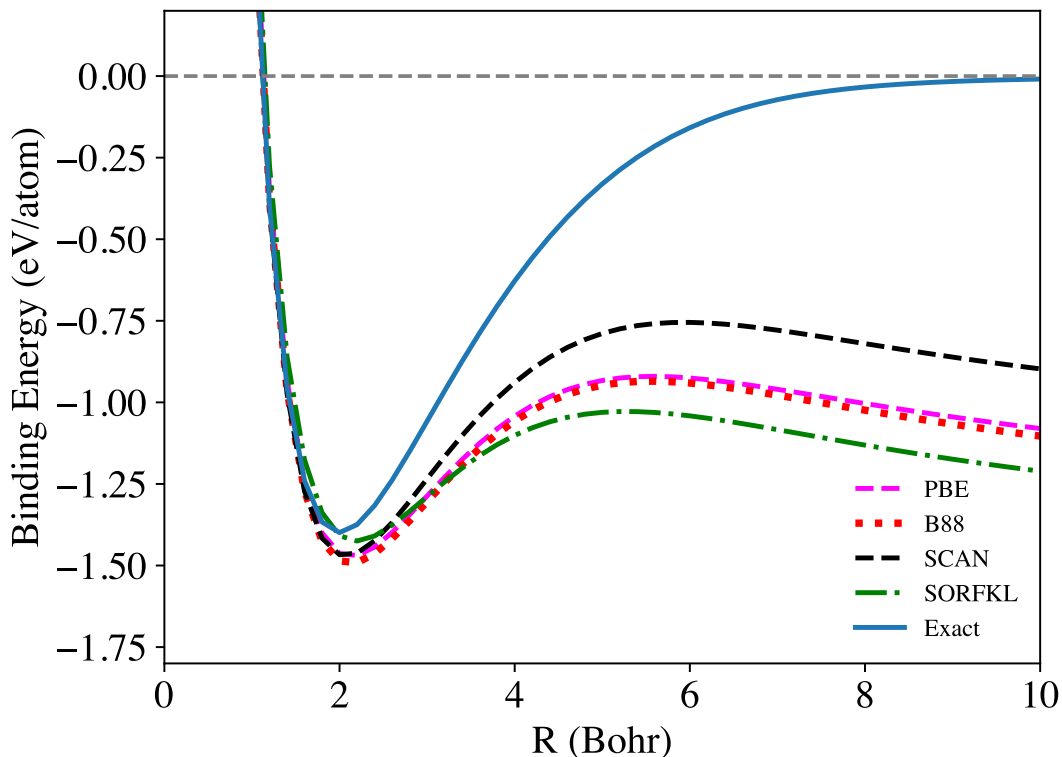


Figure S5. The binding energy curves of H_2^+ evaluated with Hartree-Fock(HF) and other exchange-only density functionals using the cc-pV5Z basis set.

* These authors contributed equally to this work

† Corresponding Author: jsun@tulane.edu

- [1] C.-O. Almbladh and U. von Barth, *Physical Review B* **31**, 3231 (1985).
- [2] N. March, *Physical Review A* **36**, 5077 (1987).
- [3] A. D. Becke, *Physical Review A* **38**, 3098 (1988).
- [4] P. Antoniewicz and L. Kleinman, *Physical Review B* **31**, 6779 (1985).
- [5] J. P. Perdew, *Physical Review Letters* **55**, 1665 (1985).
- [6] E. Gross and R. Dreizler, *Zeitschrift für Physik A Atoms and Nuclei* **302**, 103 (1981).
- [7] M. Brack, B. Jennings, and Y. Chu, *Physics Letters B* **65**, 1 (1976).
- [8] J. W. Furness, A. D. Kaplan, J. Ning, J. P. Perdew, and J. Sun, *The Journal of Chemical Physics* **156**, 034109 (2022).
- [9] J. Sun, J. P. Perdew, and A. Ruzsinszky, *Proceedings of the National Academy of Sciences* **112**, 685 (2015).
- [10] K. V. Price, R. M. Storn, and J. A. Lampinen, *Differential evolution: a practical approach to global optimization*, 37 (2005).
- [11] P. Virtanen, R. Gommers, T. E. Oliphant, M. Haberland, T. Reddy, D. Cournapeau, E. Burovski, P. Peterson, W. Weckesser, J. Bright, *et al.*, *Nature methods* **17**, 261 (2020).
- [12] E. Clementi and C. Roetti, *Atomic data and nuclear data tables* **14**, 177 (1974).
- [13] J. Furness and S. Lehtola, code repository available at <https://github.com/JFurness1/AtomicOrbitals> (2021).
- [14] J. Sun, A. Ruzsinszky, and J. P. Perdew, *Physical Review Letters* **115**, 036402 (2015).
- [15] J. Tao, V. N. Staroverov, G. E. Scuseria, and J. P. Perdew, *Physical Review A—Atomic, Molecular, and Optical Physics* **77**, 012509 (2008).
- [16] F. Jorge and M. Franco, *Chemical Physics* **253**, 21 (2000).
- [17] D. G. Smith, L. A. Burns, A. C. Simmonett, R. M. Parrish, M. C. Schieber, R. Galvelis, P. Kraus, H. Kruse, R. Di Remigio, A. Alenaizan, *et al.*, *The Journal of Chemical Physics* **152** (2020).
- [18] E. W. Lemmon, M. L. Huber, M. O. McLinden, *et al.*, *Reference fluid thermodynamic and transport properties (REFPROP)*, version **9** (2010).
- [19] T. H. Dunning Jr, *The Journal of Chemical Physics* **90**, 1007 (1989).
- [20] A. K. Wilson, T. Van Mourik, and T. H. Dunning Jr, *Journal of Molecular Structure: THEOCHEM* **388**, 339 (1996).
- [21] J. Pitarke and A. Eguiluz, *Physical Review B* **63**, 045116 (2001).
- [22] J. Sun, B. Xiao, Y. Fang, R. Haunschild, P. Hao, A. Ruzsinszky, G. I. Csonka, G. E. Scuseria, and J. P. Perdew, *Physical Review Letters* **111**, 106401 (2013).
- [23] O. A. Vydrov and T. Van Voorhis, *Physical Review Letters* **103**, 063004 (2009).
- [24] A. Ramasamy, L. Hou, J. V. Bazantes, T. J. Irons, A. M. Wibowo-Teale, T. Lebeda, and J. Sun, *Physical Review B* **112**, L161112 (2025).